Material-specific imaging of nanolayers using extreme ultraviolet coherence tomography: supplementary material

FELIX WIESNER[1,2,*], MARTIN WÜNSCHE[1,2], JULIUS REINHARD[1,2], JOHANN JAKOB ABEL[1], JAN NATHANAEL[1,2], SLAWOMIR SKRUSZEWICZ[1], CHRISTIAN RÖDEL[5], SERGIY YULIN[3], ANNETT GAWLIK[4], GABRIELE SCHMIDL[4], UWE HÜBNER[4], JONATHAN PLENTZ[4], GERHARD G. PAULUS[1,2], AND SILVIO FUCHS[1,2]

[1] *Institute of Optics and Quantum Electronics, Friedrich Schiller University Jena, Jena, Germany*
[2] *Helmholtz Institute Jena, Jena, Germany*
[3] *Fraunhofer Institute for Applied Optics and Precision Engineering (IOF), Jena, Germany*
[4] *Leibniz Institute of Photonic Technology (IPHT), Jena, Germany*
[5] *Institute of Nuclear Physics, Technical University of Darmstadt, Darmstadt, Germany*
[*] *Corresponding author: felix.wiesner@uni-jena.de*

Compiled February 22, 2021

This document provides supplementary information to "Material-specific imaging of nanolayers using extreme ultraviolet coherence tomography," https://doi.org/10.1364/OPTICA.412036.

1. WINDOW FUNCTION IN SPECTRAL DOMAIN

A direct calculation of the XCT depth structure, $\mathfrak{r}(z)$, from the measured reflectivity, $r(\kappa_D)$, leads to strong Fourier artifacts. These are caused by steep edges at the upper and lower boundaries of the measured spectrum, $\kappa_{D,\max}$ and $\kappa_{D\min}$. For suppression of these artifacts, a window function,

$$W(\kappa_D) = \begin{cases} \dfrac{\mathfrak{I}_0\left[\beta\sqrt{1-\left(\frac{2(\kappa_D-\gamma)}{\eta}\right)^2}\right]}{\mathfrak{I}_0(\beta)} & \text{for} \quad \kappa_{D,\min} \le \kappa_D \le \kappa_{D,\max} \\ 0 & \text{else} \end{cases} \tag{S1}$$

is used. Here, $\mathfrak{I}_0$ is the modified Bessel function of the first kind, $\eta = \kappa_{D,\max} - \kappa_{D,\min}$ the bandwidth, $\gamma = (\kappa_{D,\max} + \kappa_{D,\min})/2$ its center. The width of the window is given by the measured range of κ_D and the damping parameter, β. Larger β means a smaller window and consequently a better suppression of artifacts but lower depth resolution. The definition of the window function in frequency domain, $W(\omega)$, is analogous to the wave vector domain.

2. FILTER FUNCTION IN THE TIME DOMAIN

As a filter function in time domain, $F_j(t)$, a rectangular function

$$F_j(t) = \begin{cases} 0, & t < t_1 \\ 1, & t_1 \le t \le t_2 \\ 0, & t > t_2 \end{cases} \tag{S2}$$

is used. The boundaries, t_1 and t_2, need to be chosen carefully to filter the reflections of single interfaces.

3. ELIMINATION OF THE SPECTRAL WINDOW FUNCTION

After performing the isolation of a single interface by a truncated Fourier transformation the spectral window function needs to be eliminated in order to obtain the interface's reflectivity. This can be achieved by simply dividing through the window function, $W(\omega)$, if some limitations are considered. The window function can be eliminated through a simple division after filtering and Fourier transformation, if

$$r_j^F(\omega) \approx r_j^{\text{eff}}(\omega) \cdot e^{i\mathcal{O}_{\omega_0}(\omega)} \cdot W(\omega). \tag{S3}$$

Actually, the filtered signal is

$$r_j^F(\omega) = \mathcal{FT}_{\omega,t}\left[F_j(t)\right] \circledast \left[r_j^{\text{eff}}(\omega)\cdot e^{i\mathcal{O}_{\omega_0}(\omega)}\cdot W(\omega)\right], \quad \text{(S4)}$$

after zero-shift and Fourier transform into ω-domain. Equation (S3) is fulfilled, if the filtering in time domain can be approximated as

$$\begin{aligned}\mathfrak{r}_j^F(t) = \frac{1}{4\pi^2}F_j(t)\cdot\Bigg[&\mathcal{FT}^{-1}_{\omega,t}\left[r_j^{\text{eff}}(\omega)\right]\circledast\delta(t)\\ &\circledast\mathcal{FT}^{-1}_{\omega,t}\left[e^{i\mathcal{O}_{\omega_0}(\omega)}\right]\circledast\mathcal{FT}^{-1}_{\omega,t}\left[W(\omega)\right]\Bigg]\\ \approx\frac{1}{4\pi^2}\Bigg[&\mathcal{FT}^{-1}_{\omega,t}\left[r_j^{\text{eff}}(\omega)\right]\circledast\delta(t)\circledast\\ &\mathcal{FT}^{-1}_{\omega,t}\left[e^{i\mathcal{O}_{\omega_0}(\omega)}\right]\circledast\mathcal{FT}^{-1}_{\omega,t}\left[W(\omega)\right]\Bigg]. \quad \text{(S5)}\end{aligned}$$

This is the case, if the convolution of the effective reflectivity, $\mathcal{FT}^{-1}_{\omega,t}\left[r_j^{\text{eff}}(\omega)\right]$, the spectral window, $\mathcal{FT}^{-1}_{\omega,t}\left[W(\omega)\right]$ and the dispersion terms, $\mathcal{FT}^{-1}_{\omega,t}\left[e^{i\mathcal{O}_{\omega_0}(\omega)}\right]$, is assumed to be negligible outside of the filter, $F_j(t)$. Such a filter function can be chosen, if the linear phase shift between interfaces is larger than these broadening terms. Consequently, the minimum distance between two interfaces that is needed to successfully perform the filtering, depends on the spectral behaviour of these interfaces. For instance, a steep absorption edge causes a broad signal in time domain, and would therefore require a large distance between adjacent interfaces. The broadening due to the spectral window, $W(\omega)$, can be controlled by choosing an appropriate damping parameter, β.

4. MODEL FOR THE LIGHT-MATTER INTERACTION

The overall, complex reflectivity, $r(\omega)$, of a sample can be written as the sum over reflections at the individual interfaces

$$r(\omega) = \sum_{j=1}^{N} r_j^{\text{eff}}(\omega)e^{i\Phi_j(\omega)}. \quad \text{(S6)}$$

Here, a phase shift, $\Phi_j(\omega)$, describes the propagation in the sample, while the effective reflectivities, $r_j^{\text{eff}}(\omega)$, contain reflection, transmission and absorption. The frequency dependency of $\Phi_j(\omega)$ and $r_j^{\text{eff}}(\omega)$ accounts for the full dispersion in the sample. Multiple reflections are neglected.

To relate the factors in equation (S6) to the refractive index distribution in the medium, the z-component of the wave-vector, κ_j, in each medium j, needs to be calculated

$$\kappa_j(\omega) = \kappa_j'(\omega) + i\kappa_j''(\omega) = \frac{2\omega}{c}\sqrt{n_j^2(\omega) - \cos^2(\alpha)}, \quad \text{(S7)}$$

where α is the angle of incidence with respect to the surface and n_j is the complex refractive index in the corresponding layer. The field reflectivity, $r(\omega)$, of the whole stack is then given by

$$\begin{aligned}r(\omega) =& r_{01}(\omega) + \quad \text{(S8)}\\ &\sum_{j=2}^{N} r_{(j-1)j}(\omega)\cdot\Bigg[\prod_{l=1}^{j-1}\underbrace{\theta_{l(l-1)}(\omega)\theta_{(l-1)l}(\omega)}_{\text{transmission}}\cdot\\ &\underbrace{e^{-2\kappa_l''(\omega)(z_{l+1}-z_l)}}_{\text{absorption}}\cdot\underbrace{e^{2i\kappa_l'(\omega)(z_{l+1}-z_l)}}_{\text{dispersion}}\Bigg].\end{aligned}$$

The transmission θ_{ij} and the reflectivity r_{ij} of the isolated interface between the layers i and j can be obtained with the Fresnel equations:

$$\begin{aligned}&\text{TE-polarization} && \text{TM-polarization}\\ &r_{ij} = \frac{\kappa_i - \kappa_j}{\kappa_i + \kappa_j} && r_{ij} = \frac{\varepsilon_j\kappa_i - \varepsilon_i\kappa_j}{\varepsilon_j\kappa_i + \varepsilon_i\kappa_j}\\ &\theta_{ij} = \frac{2\kappa_i}{\kappa_i + \kappa_j} && \theta_{ij} = \frac{\sqrt{4\varepsilon_i\varepsilon_j}\kappa_i}{\varepsilon_j\kappa_i + \varepsilon_i\kappa_j}, \quad \text{(S9)}\end{aligned}$$

where ε_j is the complex susceptibility of the medium j. The index $i = 0$ denotes the medium on top of the sample, i.e. its cladding, whereas index N indicates the substrate.

By comparing equations (S6) and (S8) one finds the equivalences

$$\begin{aligned}&\Phi_1(\omega) = 0 \quad , \quad \Phi_{j>1}(\omega) = \sum_{l=1}^{j-1} 2\kappa_l'(\omega)(z_{l+1} - z_l) \quad \text{(S10)}\\ &r_1^{\text{eff}}(\omega) = r_{01}(\omega)\\ &r_{j>1}^{\text{eff}}(\omega) = r_{(j-1)j}(\omega)\prod_{l=1}^{j-1}\theta_{l(l-1)}(\omega)\theta_{(l-1)l}(\omega)e^{-2\kappa_l''(\omega)(z_{l+1}-z_l)}.\end{aligned}$$

The phase, Φ_j, is the sum over the propagation in all layers on top of the interface with the distance z_j to the surface.

If the wave-vector in all media is now approximated by the wave vector κ_D in the dominant medium, the phase term simplifies to $\Phi_j = \kappa_D z_j$.

Interface roughness can be introduced by the Nevot-Croce Factor [1]

$$\rho_{(j-1)j} = e^{-2\kappa_{j-1}\kappa_j\sigma_j^2}. \quad \text{(S11)}$$

The roughness is given by the root-mean-square value σ_j of the interface. Roughness is included in the model by replacing the reflectivity of the plain surface, $r_{(j-1)j}$, in equation (S10) with the reflectivity of the rough surface:

$$r_{(j-1)j}^{\text{rough}} = \rho_{(j-1)j}r_{(j-1)j} \quad \text{(S12)}$$

5. CALCULATION OF THE SAMPLE REFLECTIVITY FROM THE MEASURED SPECTRUM

The sample reflectivity, R, is calculated from four measured reflection spectra. A sketch of this data processing is shown in figure S1. The measured spectrum, S_{M}, is the product of the sample reflectivity, R, and the source spectrum, S_{Source}. It follows:

$$R = \frac{S_M}{S_{\text{Source}}}. \quad \text{(S13)}$$

The source spectrum is obtained by measuring the reflected spectrum of a reference material, S_{ref}, with known reflectivity, R_{ref}:

$$S_{\text{source}} = \frac{S_{\text{ref}}}{R_{\text{ref}}}. \quad \text{(S14)}$$

The reflected spectrum of the sample and the reference is measured for two different filter configurations, in order to extend the measurable spectral region of XCT. The spectral region covered in a single exposure is defined by the transmission bandwidth of the transmission filter used. For our experiment Al and

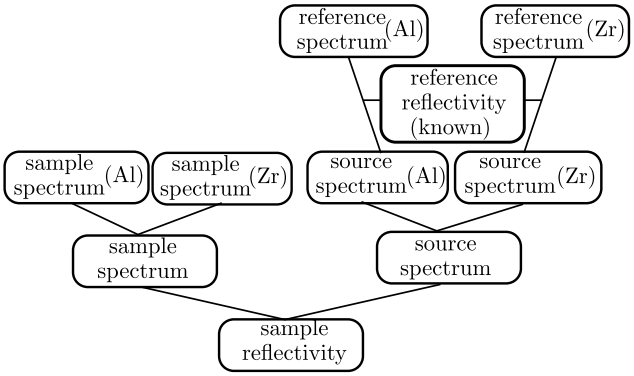

Fig. S1. Sketch of the calculation of the sample reflectivity from four measured spectra: The sample is measured with two complementary filter configurations (Al and Zr). These are combined to cover a broad spectral range. The source spectrum is characterized by a reference measurement at a material with known reflectivity. In our case we used TiO_2 as a reference and calculated the reflectivity with dispersion data from [2]. The sample reflectivity is calculated according to equation (S13).

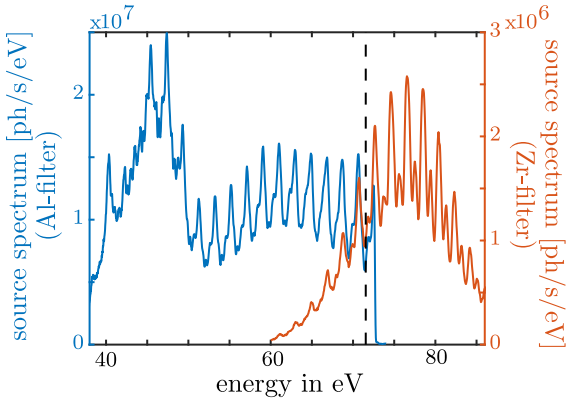

Fig. S2. The source spectrum obtained with aluminum (blue) and zirconium (red). Here, the source spectrum is defined as the spectrum incident on the sample, which includes the transmission through the filters. Consequently, an offset between the spectra is observed, due to the different filter apertures and transmissions. The black dotted line shows at which photon energy the two spectra are merged.

Zr transmission filters provide complementary transmission windows. The source spectrum for both filter configurations is shown in figure S2. The spectrum is quasi-continuous, but still contains modulations from the high harmonic generation process. The offset between the two parts is caused by the different filter transmissions and apertures. The source spectrum, S_{Source}, and the sample spectrum, S_{Sample}, are obtained by merging the spectra obtained for the different filter configurations. They are shown for sample 1 (buried Ti and SiO2 layers in silicon) in figure S3a). When the sample reflectivity, R, is calculated according to equation (S13), the contribution of the different filter transmissions cancel out. The sample reflectivity for sample 1 is shown in figure S3b).

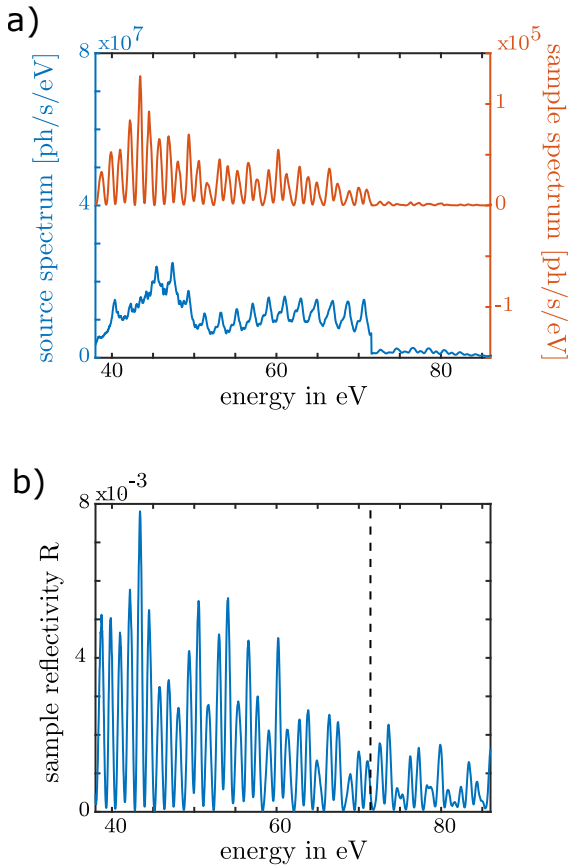

Fig. S3. a) Source spectrum (blue) and sample spectrum (red) of sample 1 in the whole usable photon energy range: The black dotted line shows were the contributions from both filter configurations are merged. **b)** The reflectivity of sample 1 is obtained from the source spectrum and sample spectrum (shown in figure a)).

6. SAMPLE DESIGN

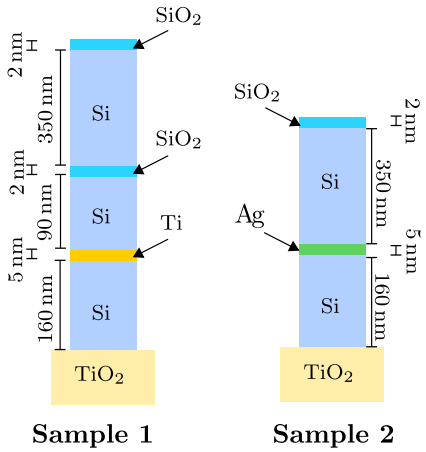

Fig. S4. Sketch of the samples: The design values for the layer thicknesses are shown. For the naturally grown silicon oxide layers, these are only estimates.

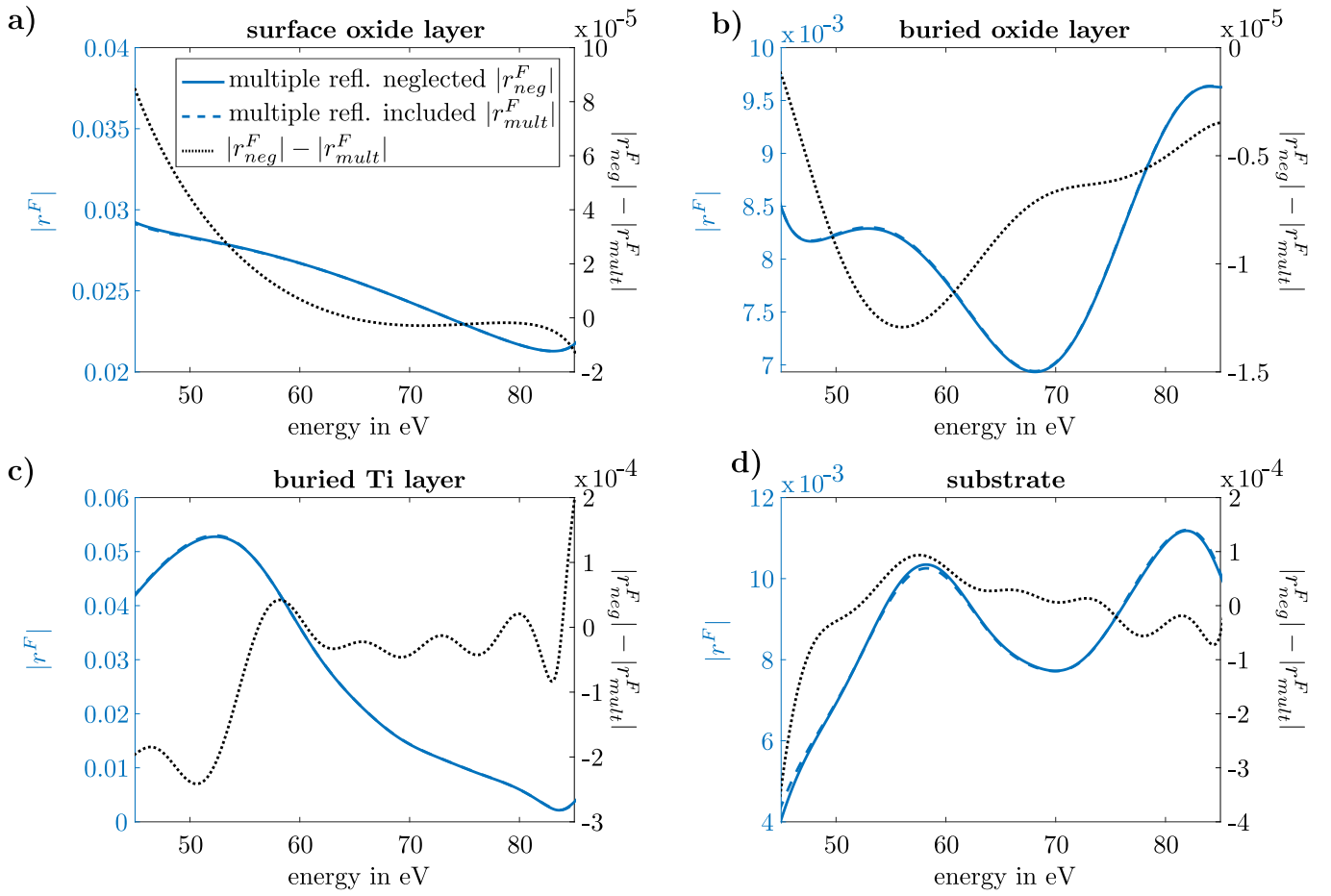

Fig. S5. The retrieved reflectivity from simulated data is shown for the cases with and without the neglection of multiple reflections inside the sample, $|r^F_{neg}|$ (solid blue) and $|r^F_{mult}|$ (dashed blue). The difference function, $|r^F_{neg}| - |r^F_{mult}|$ is shown in dotted black. The simulated structure corresponds to the design of sample 1 (figure S4) without assuming any interface roughness.

7. MULTIPLE REFLECTIONS

In the model presented in section 4 of this supplementary, multiple reflections inside of samples are neglected. This assumption was tested by performing the algorithm described in section 2.B on simulated data with and without including multiple reflections. The design structure of sample 1 was used for this purpose (see figure S4). No roughness was assumed, since this would decrease the interface reflectivity and therefore the relative weight of multiple reflections. Consequently, an upper limit for the contributions of multiple reflections was obtained. Figure S5 shows the filtered effective reflectivities retrieved from simulated data assuming multiple reflections inside the sample, r^F_{mult}, and neglecting multiple reflections, r^F_{neg}. For the simulation with multiple reflections the transfer-matrix formalism for stratified media was used [3]. For the simulation neglecting multiple reflections, the reflectivity was calculated according to equation S6. The difference between the two cases, $|r^F_{neg}| - |r^F_{mult}|$ is also shown for each structure. The deviation is generally higher at lower photon energies, but is typically 2-3 orders of magnitude smaller than the retrieved reflectivities. Consequently, the neglection of multiple reflections is reasonable for the investigated samples.

8. THE EFFECTIVE REFLECTIVITY FOR A SUPERPOSITION OF INTERFACES

The superposition of two adjacent interfaces r^{eff}_j and r^{eff}_{j+1} can be treated as a single interface. Following equations (S6) and (S10), the reflection of this single interface, $r^{\text{eff}}_{j'}$, can be described as

$$\begin{aligned} &r^{\text{eff}}_j e^{i\Phi_j(\omega)} + r^{\text{eff}}_{j+1} e^{i\Phi_{j+1}(\omega)} \\ &= \underbrace{\left(r^{\text{eff}}_j + r^{\text{eff}}_{j+1} e^{i2\kappa'_{j+1}(\omega)(z_{j+1}-z_j)}\right)}_{r^{\text{eff}}_{j'}} e^{i\Phi_j(\omega)}. \end{aligned} \tag{S15}$$

The associated propagation phase is the one corresponding to the first of the two interfaces, Φ_j.

9. REPEATABILITY

In the following, the repeatability of the algorithmic reconstruction of the filtered effective layer reflectivities, $r^F(\omega)$, is studied. Here, the major challenge is the stability of the phase retrieval of the sample structure. As explained in [4] and its supplementary, the phase-retrieval is a three-step algorithm with a random initial phase guess. All three steps rely on iterations between frequency and time domain using Gerchberg-Saxton [5] and Hybrid-Input-Output [6] constraints, which are well established

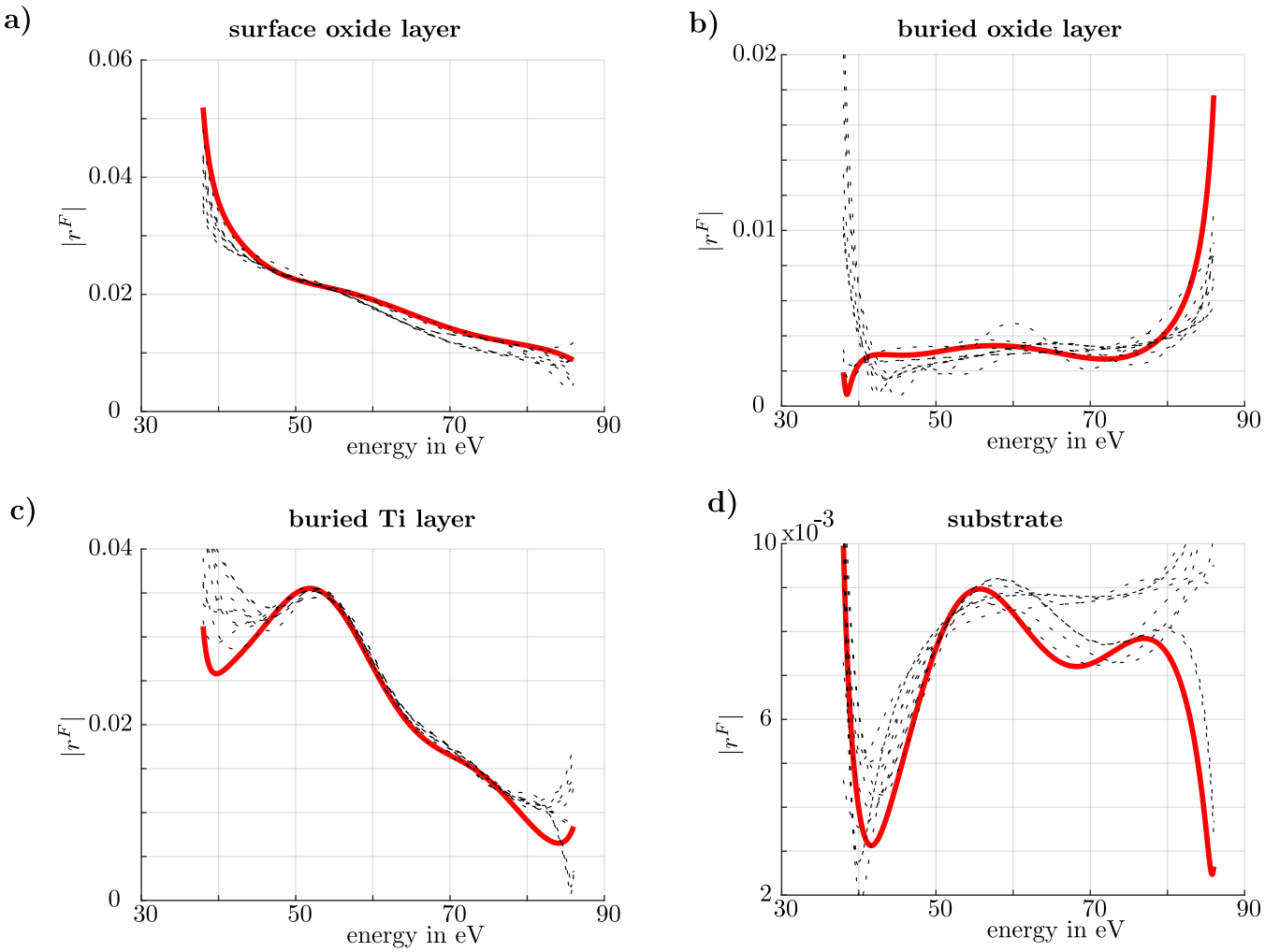

Fig. S6. Repeatability of the measurement: The results for multiple phase retrieval runs are shown (dotted black).For further analysis and the comparison to the simulated data, the results with the smallest phase retrieval error were chosen.

for the case of two-dimensional phase retrieval. Because of the lack of symmetries in the measured one-dimensional signal, the direct application of these constraints will not lead to convergence. Therefore, tighter constraints are initially applied in both domains to obtain an initial guess for the amplitude in the depth domain. The additional constraints are then loosened stepwise, ultimately yielding the complex signal in the time and frequency domain, with a compact support as the only constraint left in the final step. In each step the convergence of the phase retrieval can be monitored using the error function

$$\mathfrak{e} = \frac{\int |r'^m_W(\omega) - r^0_W(\omega)|^2 \mathrm{d}\omega}{\int |r^0_W(\omega)|^2 \mathrm{d}\omega}, \tag{S16}$$

where $r'^m(\omega)$ is the amplitude in spectral domain after the m-th iteration and

$$r^0_W(\omega) = \begin{cases} r_{ww_{sym}}(\omega), \text{ step 1} \\ W(\omega) \cdot \sqrt{R(\omega)}, \text{ step 2 and 3} \end{cases} \tag{S17}$$

the input value of the amplitude for each step. This corresponds to a symmetrization of the input spectrum, $r_{ww_{sym}}(\omega)$, for step 1 and the square root of the measured intensity reflectivity, $R(\omega)$ for step 2 and 3, weighted with the window function $W(\omega)$. In the original work by Fuchs et al. the phase retrieval was found to provide a stable reconstruction of the sample structure. This is achieved by running the phase retrieval multiple times and selecting the result with the minimal error, $\mathfrak{e}$, to neglect cases where the algorithm converges to the wrong solution due to the initial random spectral phase. The current work is even more senstitive to the result of the phase retrieval, because the reflectivity of individual interfaces is investigated in addition to the spatial sample strucuture. To discuss the repeatability of this approach , the results for the filtered effective reflectivity, r^F, for eleven phase retrieval runs are shown for sample 1 in figure S6. The red curves show the reconstructed reflectivities with the lowest phase retrieval error and are the ones used for the discussion and comparison to simulated data in the manuscript. The deviation between subsequent runs is highest for the interfaces with a low reflectivity. Additionally, deviations occur predominantly at the edges of the spectral range. Consequently, the deviations can be attributed to the presence of noise in the retrieved sample structure, $\mathfrak{r}(t)$. This leads to errors for the interfaces with the lowest signal-to-noise ratio, i.e., the lowest reflectivity, and to stronger Fourier transform artifacts in the Fourier filtering procedure. A more stable source and a better reference measurement of the source spectrum will enable better signal-to-noise ratios

and therefore also would lead to an improved repeatability of the algorithmic reconstruction.

10. SPECTRAL RESOLUTION

The spectral resolution of the retrieved spectral reflectivity of each layer is defined by the width of the filter in time domain. Theoretically this is limited by the distance between two adjacent interfaces. In the current state, very tight filter constraints turned out to be necessary in order to prevent distortions of the reconstructed spectral reflectivity due to noise in the time domain. Table S1 shows the width of the filter used for each interface and the resulting spectral resolution. Here, the resolution is defined as the Full-Width-Half-Maximum (FWHM) of the Fourier transform of the filter function. In adddition, we investigated the best possible spectral resolution for each interface of each sample. For this purpose we simulated the samples with the matrix method and found the maximum filter width and its corresponding spectral resolution, which is referred to as theoretical resolution. These are also shown in table S1.

Table S1. The resolution of the effective reflectivity, $r^{\mathrm{eff}}(\omega)$, are shown for each reconstructed structure. For comparison, the maximum theoretical resolution that can be achieved for each structure is also computed and shown here.

Structure		exp. resolution in eV	theor. resolution in eV
Sample 1:	SiO_2	9.3	1.2
	SiO_2	12.2	7.1
	Ti	7.5	4.0
	TiO_2	9.4	3.0
Sample 2:	SiO_2	14.1	1.2
	Ag	8.2	3.7
	TiO_2	6.3	2.7

REFERENCES

1. L. Névot and P. Croce, "Caractérisation des surfaces par réflexion rasante de rayons X. Application à l'étude du polissage de quelques verres silicates," Revue de Physique Appliquée **15**, 761–779 (1980).
2. B. L. Henke, E. M. Gullikson, and J. C. Davis, "X-ray interactions: photoabsorption, scattering, transmission and reflection E= 50-30,000 eV, Z= 1-92," At. data nuclear data tables **54**, 181–342 (1993).
3. M. Born and E. Wolf, *Principles of optics: Electromagnetic theory of propagation, interference and diffraction of light* (Cambridge University Press, 1997).
4. S. Fuchs, M. Wünsche, J. Nathanael, J. J. Abel, C. Rödel, J. Biedermann, J. Reinhard, U. Hübner, and G. G. Paulus, "Optical coherence tomography with nanoscale axial resolution using a laser-driven high-harmonic source," Optica **4**, 903–906 (2017).
5. R. W. Gerchberg, "A practical algorithm for the determination of phase from image and diffraction plane pictures," Optik **35**, 237–246 (1972).
6. J. R. Fienup, "Reconstruction of an object from the modulus of its Fourier transform," Opt. Lett. **3**, 27 (1978).